Competing Magnetic Phases on a Kagomé Staircase

G. Lawes,[1] M. Kenzelmann,[2,3] N. Rogado,[4] K. H. Kim,[1,*] G. A. Jorge,[1] R. J. Cava,[4] A. Aharony,[5] O. Entin-Wohlman,[5] A. B. Harris,[6] T. Yildirim,[3] Q. Z. Huang,[3] S. Park,[3,7,†] C. Broholm,[2,3] and A. P. Ramirez[1,8]

[1]*Los Alamos National Laboratory, Los Alamos, NM 87544, USA*
[2]*Department of Physics and Astronomy, Johns Hopkins University, Baltimore, MD 21218, USA*
[3]*NIST Center for Neutron Research, Gaithersburg, MD 20899, USA*
[4]*Department of Chemistry and Princeton Materials Institute, Princeton University, Princeton, NJ 08544, USA*
[5]*School of Physics and Astronomy, Raymond and Beverly Sackler Faculty of Exact Sciences, Tel Aviv University, Tel Aviv 69978, Israel*
[6]*Department of Physics and Astronomy, University of Pennsylvania, Philadelphia, PA, 19104, USA*
[7]*Department of Materials Science and Engineering, University of Maryland, College Park, MD 20742, USA*
[8]*Bell Labs, Lucent Technologies, 600 Mountain Avenue, Murray Hill, NJ 07974, USA*

(Received 12 July 2004; published 7 December 2004)

We present thermodynamic and neutron data on $Ni_3V_2O_8$, a spin-1 system on a kagomé staircase. The extreme degeneracy of the kagomé antiferromagnet is lifted to produce two incommensurate phases at finite T—one amplitude modulated, the other helical—plus a commensurate canted antiferromagnet for $T \to 0$. The H-T phase diagram is described by a model of competing first and second neighbor interactions with smaller anisotropic terms. $Ni_3V_2O_8$ thus provides an elegant example of order from subleading interactions in a highly frustrated system.

DOI: 10.1103/PhysRevLett.93.247201 PACS numbers: 75.10.Jm, 75.25.+z, 75.30.Kz

Geometrical magnetic frustration leads to unusual low temperature spin order and dynamics and presents new challenges for the theoretical understanding of magnetic systems. Frustrated materials are often characterized by triangle-based lattices and short-range antiferromagnetic (AF) interactions [1]. Of particular interest has been magnetism on the two-dimensional (2D) kagomé lattice, which consists of corner-sharing triangles. While the Heisenberg spin-1/2 model appears to have short-range spin correlations and a gap to free spinons [2,3], the $S \to \infty$ classical model has Néel order with a $\sqrt{3} \times \sqrt{3}$ unit cell at temperature $T = 0$ [4]. Materials that approximate the kagomé AF can be expected to lie close to a quantum critical point, and indeed early work on the kagomé system $SrCr_{9p}Ga_{12-9p}O_{19}$ exposed a spin liquid phase possessing a large fraction (15%) of the total spin entropy and short-range $\sqrt{3} \times \sqrt{3}$ order [5,6]. Later work on jarosite systems showed different "$q = 0$" long range order apparently favored by interlayer interactions[7].

Here we study $Ni_3V_2O_8$ (NVO) in which the $S = 1$ Ni^{2+} spins form the orthorhombic kagomé staircase structure shown in Fig. 1(a) [8]. This structure has the coordination and two dimensionality of the regular kagomé lattice, but the kagomé planes are buckled. The system is particularly attractive because its complex magnetic phase diagram can be understood on the basis of an embellished kagomé spin Hamiltonian. The model we introduce also applies to the isostructural compounds where Ni is replaced by Cu [9] or Co [10]. Although the symmetry of these compounds is the same as that of NVO, their phase diagrams are very different. As indicated below, this difference results from a small quantitative change in the parameters which dictate how frustration is relieved.

A previous study of the magneto-thermal response in polycrystalline NVO revealed four zero field phase transitions with $\Theta_W/T_N > 5$, where Θ_W is the Weiss constant and T_N the magnetic ordering temperature [10]. In this Letter we report an unexpectedly rich anisotropic field-temperature (H-T) phase diagram (Fig. 2), with high and low temperature incommensurate (IC) phases (HTI and LTI) and two commensurate (C and C′) spin structures. These magnetic structures are determined via neutron diffraction. We also explain the salient features of NVO by a model, in which the spine (Ni_s) and cross-tie (Ni_c) spins interact via nearest-neighbor (NN) and second nearest-neighbor (SNN) isotropic Heisenberg interactions. In addition, it is necessary to take account of the Dzyaloshinskii-Moriya (DM) interaction and magnetic anisotropy.

Symmetry is key to understanding the ordered phases that spring from the kagomé critical state in NVO [11]. In the presence of AF ordering on the spine sites, isotropic NN interactions produce zero mean field on cross-tie sites. In this regard, NVO is reminiscent of $Sr_2Cu_3O_4Cl_2$ [12] and of some "ladder" systems of recent interest [13]. However, the structural anisotropy of NVO induces interactions not usually considered in frustrated systems. First, because the NiO_6 octahedra are edge-sharing, the NN Ni-O-Ni bond angle is close to 90° so the NN and SNN Ni-Ni interactions are weak and similar in strength. Second, the symmetry of the crystal structure admits a DM interaction among the NN spine spins [12]. Third, anisotropic pseudodipolar (PD) exchange interactions between spine and cross-tie spins induce both a uniform and a staggered moment on the cross-tie sites [14]. These interactions add to the usual isotropic NN superexchange

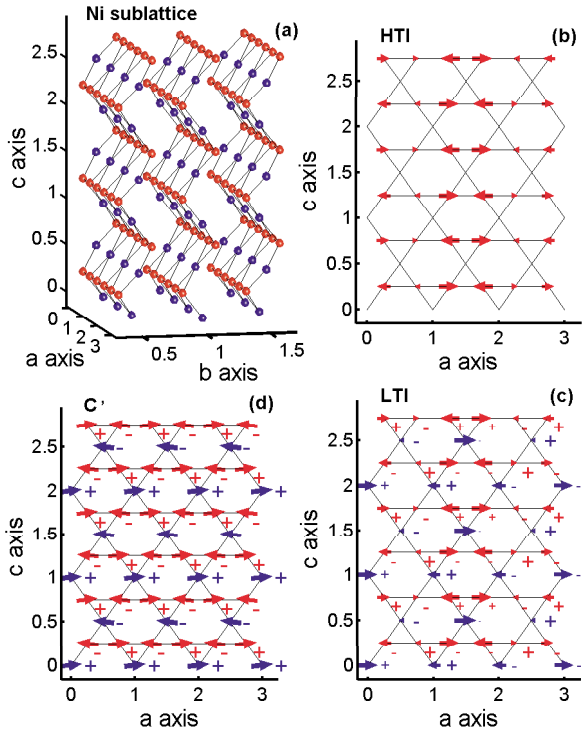

FIG. 1 (color). (a) Structure of NVO, showing the cross-tie Ni_c [blue (gray)] and spine Ni_s [red (black)] sites. (b)–(c) indicate the spin structures in the IC phases. +/− indicate spin components along **b**. Symbol sizes scale with the dipole moment. (d) indicates the symmetry of the C' structure. Spin canting has been exaggerated for clarity and the relative symbol sizes for spine and cross-tie spins are not to scale. Subsequent layers are displaced by $(\mathbf{a}+\mathbf{b})/2$ with spine spins satisfying Eq. (1). Lattice parameters serve as axis length units.

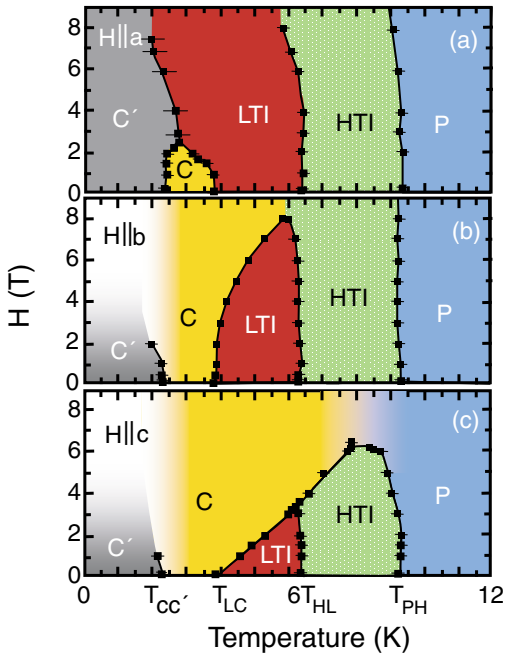

FIG. 2 (color). Phase diagram for NVO as a function of temperature and magnetic field applied along the three principal crystallographic directions. For $\mathbf{H} \parallel \mathbf{c}$ no true phase boundary separates the P and C phases. White areas were not probed.

interaction to produce the observed rich H-T phase diagram.

Single crystals of NVO were grown from a BaO-V_2O_5 flux and powder samples were synthesized with standard techniques [10,14]. The uniform magnetization, M, was probed using a SQUID magnetometer. The specific heat, C, was measured using the relaxation method for $T > 2$ K and the semiadiabatic method for lower T. Powder and single crystal neutron diffraction measurements were carried out at the NIST Center for Neutron Research [14]. The space group of NVO is Cmca (No. 64)[8] with lattice parameters $a = 5.921\,97(3)$ Å, $b = 11.372\,13(7)$ Å, and $c = 8.224\,95(5)$ Å at $T = 1.5$ K. Throughout, we index wave vectors in the orthorhombic reciprocal lattice with $a^* = 2\pi/a$, $b^* = 2\pi/b$, and $c^* = 2\pi/c$. Representative specific heat data are in Fig. 3(a) for a magnetic field (H) of 0, 5, and 8 T along c. As in previous zero field measurements on powder samples, there are four peaks in $C(T)$[10]. The entropy reduction associated with these phase transitions is determined by $\Delta S = \int_0^{50\mathrm{K}} (C/T)dT$, after subtracting an estimate of the lattice contribution obtained from the nonmagnetic structural analog $Zn_3V_2O_8$. We find $\Delta S \approx 7.9$ J/mole K, or 87% of Rln3, which is close to that expected for ordering among spin-1 Ni^{2+} ions. We infer that the specific heat peaks mark phase transitions to unique structures involving the Ni^{2+} spin-1 degrees of freedom. The $H = 0$ peaks at 2.2, 6.3, and 9.1 K indicate second order phase transitions, whereas the 3.9 K peak marks a first order transition.

Through extensive specific heat measurements, we determined the phase boundaries shown in Fig. 2. These were confirmed by susceptibility (χ) and magnetization (M) data [see Fig. 3(b)], which provide additional clues to the nature of the phases. As T is reduced and the C phase is entered, there is a sharp jump in M, up to 3.5% of the Ni^{2+} saturation moment for $\mathbf{H} \parallel \mathbf{c}$, which indicates a weak ferromagnetic (FM) moment along **c**. With $\mathbf{H} \parallel \mathbf{a}$, there is a sharp drop in M. Finally, for $\mathbf{H} \parallel \mathbf{b}$, there is no sharp feature indicating no FM moment along **b**. A surprising result of this study is that the T_{PH} and T_{HL} transitions do not produce observable anomalies in $\chi(T)$. In a field of 0.1 T, the magnetization anomaly at T_{PH} is less than 4×10^{-5} μ_B/Ni or 0.3% of the signal while it is less than 4×10^{-6} μ_B/Ni or 0.03% at T_{HL}. Nonlinear susceptibility measurements likewise produced no indication of these phase transitions.

Neutron diffraction, however, reveals T dependent magnetic Bragg peaks at $\mathbf{Q} = (2n+1 \pm q/a^*, 2m+1, 0)$ and $\mathbf{Q} = (2n+1 \pm q/a^*, 2m+1, 2m+1)$ for $T_{LC} < T < T_{PH}$. The peaks are resolution limited, indicating a correlation length in excess of 500 Å. The T dependence of the peak intensities is shown in Fig. 3(c). Anomalies are

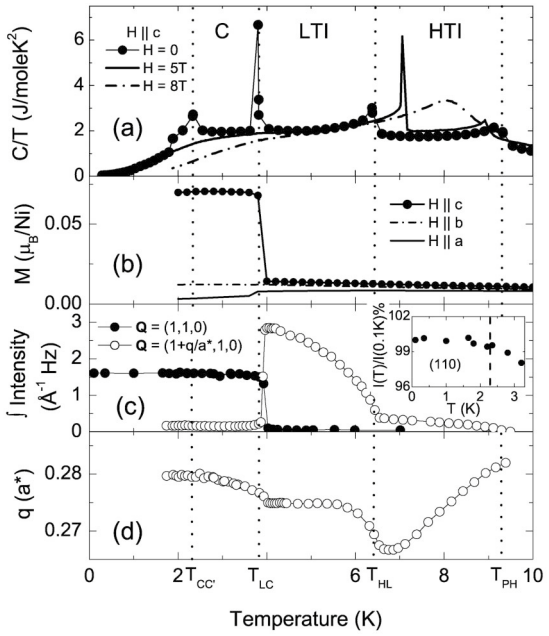

FIG. 3. (a) Specific heat of NVO, in zero field and for $\mathbf{H} \parallel \mathbf{c}$. (b) Longitudinal magnetization versus T for $H = 0.1$ T along the three principal crystallographic directions. (c) Integrated intensity of commensurate and incommensurate magnetic Bragg peaks at $\mathbf{Q} = (110)$ and $(1 \pm q/a^*, 1, 0)$, respectively. (d) Temperature dependence of the incommensurate magnetic wave vector. In the C and C′ phases, we believe the incommensurate peak reflects a metastable minority phase as it is only present after cooling through the HTI and LTI phases and can be fully suppressed by field cycling.

apparent at the three high T transitions, T_{PH}, T_{HL}, and T_{LC}, and the peaks vanish in the $H = 0$ paramagnetic (P) phase. The absence of an anomaly to the level of 0.5% (see inset) in the T dependence of the (110) magnetic Bragg peak through $T_{CC'}$ indicates that this transition involves degrees of freedom that are decoupled from the prevailing AF order. Figure 3(b) shows that the weak FM moment is also unchanged through this transition. Nonetheless, we believe the specific heat anomaly at $T_{CC'}$ is intrinsic as it was observed in all samples studied (one powder and five crystals).

The T dependence of the characteristic magnetic wave vector, q, is shown in Fig. 3(d). Again there are anomalies at all the upper transitions but not at $T_{CC'}$. In phases HTI and LTI, q varies continuously, indicative of an IC magnetic structure. The C phase is commensurate though cooling through phases HTI and LTI yields a metastable remnant of the IC modulation. To determine the spin structures in the HTI, LTI, and C′ phases, we collected zero field (ZF) magnetic Bragg intensity data for 170 peaks in the $(hk0)$ and (hkk) planes at $T = 7$ K, 5 K, and for 70 peaks at $T = 0.1$ K after ZF cooling. We analyzed the data using group theoretical classification of the possible spin structures [15].

In the HTI phase, we limited consideration to magnetic structures that form a single irreducible representation of the corresponding space group, because we reject the possibility of a multicritical point [15]. Irreducible representation Γ_4 provides an excellent account of the HTI phase with a reliability coefficient $R = 19\%$. The corresponding magnetic structure is illustrated in Fig. 1(b). At $T = 7$ K the wavelength of the a-modulated structure is $\lambda_m = 2\pi/(a^\star - q) = 1.37(1)a$ with an amplitude vector $\mathbf{m}_s^4 = [1.93(5), 0.20(5), 0.10(4)]\ \mu_B$ for spine spins and $\mathbf{m}_c^4 = [0, -0.2(2), 0.0(2)]\ \mu_B$ for cross-tie spins.

The LTI phase contains an additional irreducible representation with a wave vector that is indistinguishable from that of the coexisting Γ_4 component. The present diffraction data are consistent with either a $\Gamma_1 + \Gamma_4$ ($\chi^2 = 2.19$) or a $\Gamma_2 + \Gamma_4$ ($\chi^2 = 2.30$) structure. The $\Gamma_1 + \Gamma_4$ structure, which features moments in the $\mathbf{a} - \mathbf{b}$ plane as for the C' phase, is shown in Fig. 1(c). For $T = 5$ K the corresponding spine amplitudes are $\mathbf{m}_s^4 = [2.0(1), 0.16(9), 0.01(5)]\ \mu_B$ and $\mathbf{m}_s^1 = [0.5(5), -0.5(1), 0.00(3)]\ \mu_B$. The cross-tie amplitude is $\mathbf{m}_c^4 = [0, -2.1(2), -0.03(9)]\ \mu_B$ with a phase shift of $0.5(1)\pi$ to $\mathbf{m}_s^4$ and $\mathbf{m}_c^1 = [0.9(5), 0, 0]\mu_B$. While the phase shifts between same site Γ_1 and Γ_4 components remain undetermined, the sizes of these components when compared to the available Ni^{2+} moment, indicate elliptical $\mathbf{a} - \mathbf{b}$ plane spirals on spine and cross-tie sites. The reliability coefficient was $R = 11\%$.

In the commensurate C' phase the data are consistent with the spin structure shown in Fig. 1(d) which corresponds to a mixture of representations Γ_1 and Γ_7. The magnetization of the spine sublattice is given by $\mathbf{m}_s^1 = [0, 0.3(1), 0]\ \mu_B$ and $\mathbf{m}_s^7 = [1.5(2)\ \mu_B, 0, \mathbf{m}_{sz}^7]$, while cross-tie sites are magnetized as follows: $\mathbf{m}_c^1 = [2.3(3), 0, 0]\ \mu_B$ and $\mathbf{m}_c^7 = [0, 0.9(2)\ \mu_B, 3M - 2\mathbf{m}_{sz}^7]$. Diffraction and magnetization data respectively show that $|\mathbf{m}_{sz}^7| \leq 0.3\ \mu_B$ and $M = 0.05\ \mu_B$. Having two active representations in C' indicates that $T_{CC'}$ could mark the admixture upon cooling of Γ_1. This scenario is, however, difficult to reconcile with the absence of an anomaly in the T dependence of the (110) Bragg intensity [inset to Fig. 3(c)].

We now turn to a theoretical interpretation of these results. First, note that the dominant AF component of the spine magnetization in all $H = 0$ phases satisfies

$$\mathbf{m}(\mathbf{r}) = -\mathbf{m}(\mathbf{r} \pm \frac{1}{2}\mathbf{b}) = -\mathbf{m}(\mathbf{r} \pm \frac{1}{2}\mathbf{c} + \delta\mathbf{b}), \quad (1)$$

where $|\delta| = 0.260\,48(6)$ [8] accounts for the kagomé plane buckling. This indicates AF interactions between neighboring spines. The spin-structure within spines is controlled by competing NN and SNN isotropic Heisenberg interactions denoted J_1 and J_2. A mean-field treatment [16] indicates that for $J_2 > |J_1|/4$, the spine Hamiltonian is minimized by a mean-field spin modulation with wave vector, q, which satisfies $\cos[(a^* - q)a/2] = -J_1/(4J_2)$. Putting aside the small T dependence of q, we deduce from the experimental value ($q \approx 0.27a^*$) in the LTI and HTI phases that $J_1 \approx 2.6J_2$. In the

presence of easy-axis anisotropy, the highest-temperature ordered phase is predicted, [16] in agreement with our experiments, to be a longitudinally modulated phase in which the spins are confined to the easy a axis. If the anisotropy field H_A is not too large ($H_A < H_1$), then, as the temperature is lowered, the longitudinally modulated phase gives way to one in which an additional transverse modulated component of spin appears, growing continuously from zero as the LTI phase is entered. This scenario is also consistent with our diffraction data. At still lower T, the diffraction data indicate a commensurate AF phase. According to mean-field theory, such a transition can occur for sufficiently large anisotropy, $H_A > H_2$ [16]. Our numerical mean-field calculations [17] show that for $J_1/J_2 = 2.6$ indeed $H_1 > H_2$, so that there is a range of anisotropy field for which mean-field theory predicts the observed sequence of ZF phase transitions.

We now discuss some of the finer details of these phases. From the M versus H data, extrapolated to $H = 0$, we find that in the C phase there is a weak ferromagnetic moment. Structural considerations show that the DM interaction for a single spine takes the form

$$\mathcal{H}_{\mathrm{DM}} = \sum_n [D_c \mathbf{c} + (-1)^n D_b \mathbf{b}] \cdot [\mathbf{S}(n) \times \mathbf{S}(n+1)], \quad (2)$$

where n labels the spins consecutively along the spine. D_b gives rise to a linear coupling between the staggered moment of the spine along **a** and the weak ferromagnetic moment of the spine along **c**. This weak FM moment can induce a FM moment along **c** on the cross-tie spins via isotropic Heisenberg exchange. In addition, such a moment on the cross-tie spins can also arise via pseudodipolar interaction between the staggered moment on the spines and a uniform moment on the cross-tie spins. Symmetry also admits a staggered g tensor along the spines, the physical origin and consequences of which are similar to DM interactions [18]. The weak ferromagnetism explains the absence of a phase boundary between the P and the C phase for $\mathbf{H}||\mathbf{c}$. In the IC phases, these interactions would give rise to modulated moments along **c**. The anisotropic interactions we invoke also generate couplings between the various IC order parameters, which result in weak T dependence of the IC wave vector [17].

Next we discuss the phase boundaries between the C phase and the IC phases. Barring a multicritical point, these must be first order transitions. For $\mathbf{H}||\mathbf{c}$ the Zeeman energy, $-HM$, of the FM moment (in the C phase) explains why the transition temperatures T_{LC} and T_{HC} increase linearly with increasing H. For $\mathbf{H} \perp \mathbf{c}$, the Zeeman energy does not appear and the phase boundary of the C phase should be quadratic in H [$T_N(H) = T_N(0) + \alpha H^2$] as it depends on the differences in the susceptibilities of the phases involved. In particular, when $\mathbf{H}||\mathbf{a}$, the longitudinal susceptibility of the C phase is small and the coefficient α is negative, disfavoring the C phase. The other phase boundaries (T_{PH} and T_{HL}) are also expected to be quadratic in H, and the experimental phase diagrams are consistent with this although for the HTI phase when **H** is along **b**, the coefficient α is unusually small. This fact is linked to the absence of anomalies in χ at the HTI phase boundaries. Both features may be a consequence of a frustrated and weakly connected spin system where phase transitions occur from a strongly correlated state with short-range AF order.

In summary, we have studied the phase diagram of the spin-1 kagomé staircase $Ni_3V_2O_8$. We find that although this phase diagram is quite complicated, it can be understood on the basis of a rather simple model which reflects the symmetry of the crystal structure. The experiments and model offer a specific example of how SNN exchange, easy-axis anisotropy, and Dzyaloshinskii-Moriya interactions can induce and control complex low temperature phases in a frustrated magnet.

We acknowledge support from the LDRD program at LANL and the U.S.-Israel Binational Science Foundation under Grant No. 2000073 for work at TAU, NIST, UPenn, and JHU. The NSF supported work at JHU through Grant No. DMR-0306940, work at Princeton through Grant No. DMR-0244254, and work at SPINS through Grants No. DMR-9986442 and No. DMR-9704257. K. H. K. is partially supported by KOSEF through CSCMR.

*CSCMR & School of Physics, Seoul National University, Seoul 151-747, S. Korea.
†HANARO Center, Korea Atomic Energy Research Institute, Daejeon, S. Korea.

[1] A. P. Ramirez, in *Handbook of Magnetic Materials*, edited by K. H. J. Buschow (Elsevier, Amsterdam, 2001), Vol. 13, p. 423.
[2] S. Sachdev, Phys. Rev. B **45**, 12377 (1992).
[3] P. Sindzingre *et al.*, Phys. Rev. Lett. **84**, 2953 (2000).
[4] D. A. Huse and A. D. Rutenberg, Phys. Rev. B **45**, 7536 (1992).
[5] A. P. Ramirez *et al.*, Phys. Rev. Lett. **64**, 2070 (1990).
[6] C. Broholm, *et al.*, Phys. Rev. Lett., **65**, 3173 (1990).
[7] S.-H. Lee *et al.*, Phys. Rev. B **56**, 8091 (1997).
[8] E. E. Sauerbree *et al.*, Acta Crystallogr. B **29**, 2304 (1973).
[9] N. Rogado *et al.*, J. Phys. Condens. Matter **15**, 907 (2003).
[10] N. Rogado *et al.*, Solid State Commun. **124**, 229 (2002).
[11] T. Yildirim *et al.*, Phys. Rev. Lett. **72**, 3710 (1994).
[12] F. C. Chou *et al.*, Phys. Rev. Lett. **78**, 535 (1997).
[13] V. Kiryukhin *et al.*, Phys. Rev. B **63**, 144418 (2001).
[14] M. Kenzelmann *et al.* (to be published).
[15] Yu. A. Izyumov, V. E. Naish and R. P. Ozerov, *Neutron Diffraction of Magnetic Materials* (Consultants Bureau, New York, 1991).
[16] T. Nagamiya, in *Solid State Physics*, edited by F. Seitz and D. Turnbull (Academic Press, New York, 1967), Vol. 20, p. 346.
[17] A. Aharony *et al.* (to be published).
[18] I. Affleck and M. Oshikawa, Phys. Rev. B **60**, 1038 (1999).